

The impact of helical flow on coronary atherosclerotic plaque development

Original

The impact of helical flow on coronary atherosclerotic plaque development / De Nisco, G.; Hoogendoorn, A.; Chiastra, C.; Gallo, D.; Kok, A. M.; Morbiducci, U.; Wentzel, J. J.. - In: ATHEROSCLEROSIS. - ISSN 0021-9150. - STAMPA. - 300:(2020), pp. 39-46. [10.1016/j.atherosclerosis.2020.01.027]

Availability:

This version is available at: 11583/2819154 since: 2020-05-04T16:00:49Z

Publisher:

Elsevier Ireland Ltd

Published

DOI:10.1016/j.atherosclerosis.2020.01.027

Terms of use:

This article is made available under terms and conditions as specified in the corresponding bibliographic description in the repository

Publisher copyright

Elsevier postprint/Author's Accepted Manuscript

© 2020. This manuscript version is made available under the CC-BY-NC-ND 4.0 license
<http://creativecommons.org/licenses/by-nc-nd/4.0/>. The final authenticated version is available online at:
<http://dx.doi.org/10.1016/j.atherosclerosis.2020.01.027>

(Article begins on next page)

1 **The Impact of Helical Flow on Coronary Atherosclerotic Plaque Development**

2
3 Giuseppe De Nisco^a, Ayla Hoogendoorn^b, Claudio Chiastra^a,

4 Diego Gallo^a, Annette M. Kok^b, Umberto Morbiducci^a, Jolanda J. Wentzel^b

5
6 ^a *PoliTo^{BIO}Med Lab, Department of Mechanical and Aerospace Engineering, Politecnico di Torino,*
7 *10129 Turin, Italy*

8 ^b *Department of Cardiology, Biomedical Engineering, Erasmus MC, 3000 CA Rotterdam, The*
9 *Netherlands*

10
11
12
13
14
15 *The final publication is available online*

16 *DOI: <https://doi.org/10.1016/j.atherosclerosis.2020.01.027>*

17
18
19
20
21
22
23 **Corresponding author:**

24 Jolanda J. Wentzel, Dr. Molewaterplein 40, 3015 GD Rotterdam, The Netherlands

25 P.O. Box 2040, 3000 CA Rotterdam, The Netherlands

26 Phone: +31107044044; Fax: +31107044720; j.wentzel@erasmusmc.nl

27 **Number of figures: 5**

28 **Abstract**

29 **Background and aims** - Atherosclerosis has been associated with near wall hemodynamics and
30 wall shear stress (WSS). However, the role of coronary intravascular hemodynamics, in particular
31 of the helical flow (HF) patterns that physiologically develop in those arteries, is rarely considered.
32 The purpose of this study was to assess how HF affects coronary plaque initiation and progression,
33 definitively demonstrating its atheroprotective nature.

34 **Methods** - The three main coronary arteries of five adult mini-pigs on a high fat diet were imaged
35 by computed coronary tomography angiography (CCTA) and intravascular ultrasound (IVUS) at 3
36 (T1, baseline) and 9.4 ± 1.9 (T2) months follow-up. The baseline geometries of imaged coronary
37 arteries (n=15) were reconstructed, and pig-specific computational fluid dynamic simulations were
38 performed. Local wall thickness (WT) was measured on IVUS images at T1 and T2, and its temporal
39 changes were assessed. Descriptors of HF and WSS nature were computed for each model, and
40 statistically compared to WT data.

41 **Results** - HF intensity was strongly positively associated with WSS magnitude ($p < 0.001$). Overall,
42 coronary segments exposed to high baseline levels of HF intensity exhibited a significantly lower
43 WT growth ($p < 0.05$), compared to regions with either mid or low HF intensity.

44 **Conclusions** - This study confirms the physiological significance of HF in coronary arteries,
45 revealing its protective role against atherosclerotic WT growth and its potential in predicting
46 regions undergoing WT development. These findings support future *in vivo* measurement of
47 coronary HF as surrogate atherosclerotic risk marker, overcoming current limitations of *in vivo*
48 WSS assessment.

49 **Keywords:** Atherosclerosis; Computational fluid dynamics; Wall shear stress; plaque progression.

50 Introduction

51 Coronary atherosclerosis is a complex and multifactorial disease, influenced by local biological,
52 biomechanical, and systemic factors [1,2]. The underlying mechanisms of the transformation from
53 a healthy to a diseased coronary artery are still incompletely understood. As a consequence, a
54 robust arsenal of predictive tools for this mostly asymptomatic disease has not been identified yet.
55 Among the biomechanical factors that promote atherosclerotic plaque onset and progression in
56 coronary arteries, local hemodynamics plays a major role [2,3]. In particular, low wall shear stress
57 (WSS) is widely recognized as an independent, albeit moderate, predictor of plaque development
58 [4,5].

59 Besides the widely investigated WSS, physiological helical flow (HF) has also been
60 hypothesized to have a relevant impact on vascular disease. HF, consisting of a helical-shaped
61 arrangement of the streaming blood (as given by the combination of translational and rotational
62 blood flow motions), is known to markedly characterize arterial hemodynamics [6-9]. The
63 physiological significance of arterial HF, in particular its atheroprotective nature, has emerged in
64 the last decade in the human aorta [6,10-12] and in the human carotid bifurcation [13-15]. All
65 those studies highlighted the role played by HF in mitigating near-wall flow disturbances, thereby
66 suppressing the area exposed to low WSS, which protects from atherosclerosis development [2].

67 Very recently, we showed the existence of distinguishable HF flow features in coronary
68 arteries. These HF features were hypothesized to be atheroprotective, as our data demonstrated a
69 strong association between HF and the luminal surface area exposed to low, proatherogenic WSS
70 [16].

71 Following these recent findings, the final goal of this study was to demonstrate the protective role
72 of HF for atherosclerotic plaque development over time. Findings from this work would contribute
73 (1) to further clarify the physiological significance of HF in coronary arteries, and (2) to the debate

74 on a possible future use of HF-based hemodynamic descriptors as *in vivo* surrogate markers of
75 WSS for diagnostic/prognostic purposes overcoming current limitations and inaccuracies related
76 to the direct measurement of WSS from *in vivo* imaging [\[17\]](#).

77 **Materials and Methods**

78 *Animal population and imaging*

79 Five adult familial hypercholesterolemia Bretoncelles Meishan mini-pigs with a mutation in the
80 low-density lipoprotein receptor (*LDLR*) (age of 34 ± 3 months, castrated male) were put on a high
81 fat diet to trigger atherosclerosis development. As described in detail elsewhere [16,18], the
82 animals underwent computed coronary tomography angiography (CCTA) and intravascular
83 ultrasound (IVUS) imaging of the three main coronary arteries (left anterior descending - LAD, left
84 circumflex - LCX, and right coronary artery - RCA). The imaging protocol was performed at 3
85 months after the start of the diet (T1, considered as the baseline in this study), and after 9.4 ± 1.9
86 months (T2). At T1, Doppler-based blood flow velocity measurements were recorded in each
87 artery at the inflow section and immediately upstream and downstream of each side branch, using
88 the ComboWire (Volcano Corp., Rancho Cordova, CA, USA). An overview of the methods is
89 provided in Figure 1. In addition, some classical risk factors were measured in the 5 investigated
90 animals including weight, leukocytes, Total cholesterol, LDL-C, HDL-C and LDL-C/HDL-C ratio.
91 The study was performed according to the National Institute of Health guide for the Care and Use
92 of Laboratory animals [19]. Ethical approval was obtained from the local animal ethics committee
93 of the Erasmus MC (EMC nr. 109-14-10).

94 *Plaque growth measurements*

95 To quantify the local wall thickness (WT), the lumen and vessel wall contour of each of the 15
96 investigated coronary arteries (5 LAD, 5 LCX and 5 RCA, Figure S1 of the Supplementary Materials)
97 were semi-automatically detected on IVUS images at T1 and at T2 using QCU-CMS software
98 (version 4.69, Leiden University Medical Centre, LKEB, Division of Image Processing), as depicted in
99 Figure 2. WT was assessed by subtracting the distance between the lumen center and the outer

100 wall contour, from the distance to the lumen contour. Plaque development over time was
101 quantified in terms of change in WT (Δ WT) between time points T1 and T2. The Δ WT was then
102 adjusted for the number of months between both time points for the individual pigs, resulting in a
103 measure of Δ WT/month. WT measurements were averaged over 3mm/45 degrees sectors of the
104 luminal surface (Figure 2) in order to capture the local effects of HF on plaque development.

105 *Computational hemodynamics*

106 The 3D geometry of coronary arteries at T1 was reconstructed by stacking segmented IVUS lumen
107 contours on the CCTA 3D centerline using Mevislab (Bremen, Germany), as described in detail
108 elsewhere [16]. Unsteady-state CFD simulations were performed on the reconstructed geometries
109 to quantify near-wall and intravascular hemodynamic features. The finite volume method was
110 used to numerically solve the governing equations of fluid motion. Blood was assumed as an
111 incompressible, homogeneous, non-Newtonian fluid. No-slip condition was assumed at the
112 arterial wall. Personalized boundary conditions were derived from individual *in vivo* velocity
113 ComboWire Doppler measurements at several locations along the vessel. The most proximal
114 measurement was used to estimate the flow rate value, prescribed as inlet boundary condition in
115 terms of time-dependent flat velocity profile. At each side branch, the measured flow ratio was
116 estimated as the difference between upstream and downstream velocity-based flow rate
117 measurements and applied as outflow condition. If flow velocity measurements were inaccurate
118 or not available, a diameter-based scaling law [20] was applied to estimate the flow ratio [16].

119 *Hemodynamic descriptors*

120 The hemodynamic descriptors considered for the analysis are listed in Figure 2 (see Table S2 of the
121 Supplementary Materials for their mathematical formulation). In short, helical flow in the 15
122 coronary artery models at T1 was assessed in terms of average helicity intensity (h_2), which gives a
123 measure of the strength of the pitch and torsion of coronary blood flow and is given by the cardiac

124 cycle- and volume-averaged value of the unsigned internal product of local velocity and vorticity
125 vectors [13]. In this work, to characterize each coronary model with a representative helicity
126 intensity value, h_2 was analyzed in the near-wall volume (i.e., defined by the outer 10% of the local
127 radius) and in the whole volume (i.e., defined by the entire local radius) of the main vessel.
128 Moreover, helicity intensity data were calculated over 3mm/45 degrees sectors, considering both
129 near-wall and entire local radius volumes. The consideration of the near-wall volume was
130 motivated by the recently observed link between HF and WSS patterns perpendicular to the
131 centerline of coronary arteries, quantified by the so-called secondary WSS [16]. In addition, the
132 local normalized helicity (LNH) [21] was adopted to visualize right- and left-handed helical fluid
133 patterns inside coronary arteries (respectively, positive and negative LNH values, [11].
134 To complement the HF characterization, the luminal distribution of time-averaged wall shear
135 stress (TAWSS) and of three descriptors of WSS multidirectionality were evaluated at baseline
136 (Figure 2, Table S2). In short, WSS multidirectionality was described considering two projections of
137 WSS vector [22]: (1) along the centerline of the artery, defining the “axial direction” (\mathbf{WSS}_{ax}); (2)
138 perpendicular to the centerline, defining the secondary direction (\mathbf{WSS}_{sc}). The \mathbf{WSS}_{ax} and \mathbf{WSS}_{sc}
139 local vectors were averaged over the cardiac cycle (Avg \mathbf{WSS}_{ax} and Avg \mathbf{WSS}_{sc} , respectively).
140 Moreover, their cycle-average magnitude was evaluated (TAWSS $_{ax}$ and TAWSS $_{sc}$, respectively). To
141 detect regions at the luminal surface where the local secondary WSS component predominates
142 over the axial one, the ratio of the secondary to axial \mathbf{WSS} magnitudes (WSS_{ratio}) was computed
143 [22]. The WSS-based descriptors were also averaged over the same 3mm/45 degrees sectors at
144 the luminal surface as WT data.

145 *Statistical analysis*

146 The existence of possible associations between WSS and HF was investigated considering the
147 average values of the WSS-based descriptors and the helicity-based descriptor h_2 over each

148 individual coronary artery. Regression analysis was used to identify relations between each pair of
149 hemodynamic descriptors and reported as Spearman correlation coefficients.

150 The analysis of the relation between plaque growth and hemodynamic descriptors was conducted
151 using the sector-based data applying a mixed model with hemodynamic descriptors as fixed
152 factors, the individual vessel as random factor to correct for clustering of the analyzed sectors per
153 vessel and the average cholesterol levels as covariate (IBM SPSS Statistics, version 24.0). The
154 values of the hemodynamic descriptors were classified as low, mid or high, based on artery-
155 specific tertile-division. Statistical significance was assumed for $p < 0.05$.

156 Results

157 Classical cardiovascular risk factors, weight, leukocytes, cholesterol, LDL-C, HDL-C and LDL-C/HDL-C
158 ratio did not significantly change over time for the investigated 5 pigs and are presented in Table
159 S1 of the Supplementary Materials.

160 *Coronary hemodynamics: general observations*

161 For each investigated coronary artery model, the distribution of the WSS-based descriptors was
162 assessed, as shown for a representative case in Figure 3 (panels A-D). A similar approach was used
163 for studying the HF features: the LNH red and blue colors indicate right-handed and left-handed
164 HF patterns, respectively. Thereby, the presence of two distinguishable counter-rotating HF
165 patterns was observed in this case (Figure 3-E) and reflects the arrangement in counter-rotating
166 helical structures in all coronary arteries.

167 Figure 3-A shows the luminal distribution of TAWSS highlighting, as expected, the presence of
168 case-specific focal low TAWSS regions located at the distal portion of the main branch.
169 Furthermore, the figure shows in the other panels (B-D) that WSS was predominantly aligned with
170 the forward flow direction (i.e., positive AvgWSS_{ax} values), which was representative for all cases.
171 Moreover, it emerged that the organization of coronary blood flow in two counter-rotating helical
172 structures, which is evident from LNH visualization, influences the near-wall hemodynamics of
173 coronary vessels. Considering the coronary artery depicted in Figure 3-D, positive/negative values
174 of AvgWSS_{sc} , indicating left-handed and right-handed directions respectively, resemble the
175 rotating direction of helical flow structures given by the LNH (Figure 3-E). In addition, the analysis
176 of the luminal distributions of the WSS_{ratio} revealed that **WSS** in the axial direction (WSS_{ax}) was
177 dominant over the **WSS** perpendicular to the vessel centerline (WSS_{sc}). In fact, the WSS_{ratio} was <1

178 over most of the lumen of all the investigated coronary arteries (around 94% of the investigated
179 luminal surface sectors, see also Figure 3-B).

180 *Link between hemodynamic variables*

181 Regression analysis revealed a significant association between the average values of the WSS-
182 based descriptors and helicity intensity h_2 of each individual coronary artery (Figure 3-F). In detail,
183 TAWSS was strongly and positively associated with both whole volume h_2 ($r=0.925$, $p<0.001$) and
184 near-wall h_2 ($r=0.629$, $p<0.01$), indicating that the higher the helicity intensity (h_2) is, the higher is
185 the TAWSS value. Moreover, positive, significant associations emerged between the whole volume
186 h_2 , and both TAWSS_{ax} ($r=0.843$, $p<0.001$) and TAWSS_{sc} ($r=0.843$, $p<0.001$). A weaker, but still
187 significant, direct association emerged between near-wall h_2 and TAWSS_{ax} ($r=0.629$, $p<0.05$). Only
188 a near-significant association was observed for the near-wall h_2 and TAWSS_{sc} ($r=0.468$, $p=0.081$).
189 These results suggest a predominant role for HF intensity in the whole intraluminal volume, rather
190 than only near-wall, in determining secondary **WSS** magnitude. Last, a direct, significant
191 association between the whole volume h_2 and WSS_{ratio} ($r=0.757$, $p<0.01$) emerged, but no
192 significant association was observed for the latter with near-wall h_2 .

193 *Link between hemodynamic variables and increase in wall thickness*

194 Overall, the 15 pig coronary arteries presented a marked increase in average WT over the follow-
195 up period (WT at T1 = 0.183 ± 0.108 mm, WT at T2 = 0.427 ± 0.313 mm; $p<0.001$).
196 Coronary sectors exposed to low TAWSS exhibited a significantly larger Δ WT per month ($0.048 \pm$
197 0.007 mm/month) compared to regions with either mid (Δ WT/month = 0.035 ± 0.007 mm/month)
198 or high (Δ WT/month = 0.027 ± 0.007 mm/month) TAWSS values (Figure 4 - top panel). The analysis
199 revealed a significant, inverse association between HF and WT progression. In particular (Figure 4 -
200 top panel), in luminal sectors where near-wall h_2 was high, significantly low WT growth rate (0.032
201 ± 0.007 mm/month) was observed, compared to luminal sectors with either mid (Δ WT/month =

202 0.037 ± 0.007 mm/month) or low ($\Delta\text{WT}/\text{month} = 0.040 \pm 0.007$ mm/month) near-wall h_2 . A similar
203 relation emerged for h_2 . Among the investigated descriptors of WSS directionality, only high
204 TAWSS_{ax} was significantly associated with lower WT progression (0.030 ± 0.002 mm/month for the
205 highest TAWSS_{ax} tertile).

206 In addition, the results of the time-specific statistical analysis are reported in Figure 4 (T1 - mid
207 panel; T2 - bottom panel). In detail, the association between h_2 and WT at T1 was only near
208 significant ($p=0.06$), while no significant association emerged between near-wall h_2 and measured
209 WT at T1 (Figure 4 - mid panel). As for WSS distribution, luminal sectors exposed to high TAWSS at
210 T1 significantly displayed the lowest T1 WT values. Similar results (but with smaller standard
211 errors), were observed for TAWSS_{ax}. However, neither TAWSS_{sc} nor WSS_{ratio} were significantly
212 associated with WT at T1. The analysis of the relations between hemodynamic descriptors at T1
213 and WT at T2 revealed similar results to those found for the overall WT growth per month
214 between T1 and T2 (Figure 4 - lower panel). In contrast to the $\Delta\text{WT}/\text{month}$ analysis, in the analysis
215 of WT at T2, luminal sectors exposed to higher TAWSS_{sc} values at T1 exhibited significantly lower
216 WT values at T2.

217 Discussion

218 *Summary of findings and their implications*

219 In the present study, we investigated the association between local hemodynamics and
220 atherosclerosis progression in a representative dataset of 15 pig coronary arteries. The study
221 highlighted the existence of a clear association between HF intensity (h_2) at baseline and plaque
222 development over time in coronary arteries. In detail, sectors at the luminal surface with the
223 lowest WT growth rate values were preceded by higher baseline values of helicity intensity,
224 suggesting a beneficial role of the HF patterns in coronary arteries. The atheroprotective role of HF
225 was confirmed when extending the analysis to WSS, a factor known to be involved in
226 atherosclerotic disease [23]. These findings confirm and strengthen our previously reported
227 associations between helicity intensity and WSS-based hemodynamic descriptors in coronary
228 arteries [16].

229 A schematic of the main findings is reported in Figure 5 to summarize the hemodynamics-related
230 mechanisms that might be involved in atherosclerotic disease progression: (1) helical blood flow
231 patterns characterized by high helicity intensity (h_2) stabilize coronary hemodynamics, thus reduce
232 flow disturbances resulting in more atheroprotective WSS levels at the luminal surface (e.g., Figure
233 3-F); (2) atheroprotective WSS values maintain endothelial cells (EC) quiescence and junctions
234 stability [3,23,24], contributing to prevent plaque initiation. The already highlighted role of low
235 WSS as predictor of plaque development in coronary vessels [3,5,24] also clearly emerged in this
236 study (Figure 4 - top panel). In detail, low baseline values of TAWSS, which are associated to a low
237 HF intensity (Figure 3-F), might trigger biological mechanisms, i.e., EC polygonal shaping, pro-
238 atherogenic genes upregulation, nitric oxide reduction inducing EC dysfunction [3,23,24],
239 promoting the atherogenic plaque onset and faster disease development.

240 In this study the commonly used multidirectional WSS metric oscillatory shear index (OSI) was not
241 analyzed since previous studies demonstrated that coronary arteries develop very low OSI values
242 [16,18]. Moreover, the already observed scarce multidirectionality of WSS in coronary vessels [16]
243 was confirmed here by assessing its axial and secondary components. The WSS_{ratio} assumed values
244 lower than 1 over most of the lumen of all the investigated coronary arteries, indicating that the
245 WSS is markedly aligned with the main flow direction (see explanatory case in Figure 3-B).
246 The association of hemodynamic quantities with WT at T1 was significant only for TAWSS and
247 TAWSS_{ax}. Eventhough plaque growth was just initiated; the plaque location showed to comply
248 with the local TAWSS. Luminal regions exposed to higher TAWSS_{sc} values were significantly
249 associated to lower WT at T2, reflecting that high (atheroprotective) values of TAWSS generally
250 result in higher values of TAWSS_{sc}.
251 Furthermore, the findings of this study serve to quantitatively explain for the first time the
252 irregular helical-shaped distribution of fatty and fibrous plaques in coronary artery reported by
253 previous ex vivo studies [25-28], and hinted at by the WT patterns shown for the representative
254 case in Figure 2, where the high WT region seems to follow a helical distribution.

255 *Limitations of the study*

256 Several limitations could weaken the findings of this study. Computational hemodynamic
257 modelling suffers from assumptions and uncertainties, such us rigid walls and absence of the
258 cardiac-induced motion of coronary arteries. However, their impact on the WSS distribution has
259 been demonstrated to be minor, especially when considering time-averaged WSS quantities [29].
260 Moreover, the findings of the study are based upon a relatively modest number of coronary artery
261 models (N=15). Nevertheless, the consideration of multiple sectors within each coronary artery
262 allowed for statistically significant relationships to emerge, capturing the links between local
263 hemodynamics, WT, and WT progression, when using a linear mixed-effects model correcting for

264 intra-vessel and cholesterol WT dependence. The here adopted division of the hemodynamic
265 variables in tertiles could be considered arbitrary. However, the lack of established threshold
266 values justifies this objective and conservative choice. Lastly, this study was carried out on a pig
267 model. However, the established similarity between pig and human coronary anatomy and
268 hemodynamics [30] supports the translation of the findings of this study to human coronary
269 arteries.

270 *Future perspectives*

271 In addition to the causative role of helical flow in determining WSS, a beneficial relation between
272 HF intensity at baseline and WT and its progression in the follow-up emerged here. Taken
273 together, these findings suggest that HF intensity may serve as a convenient and pragmatic
274 surrogate marker of low WSS for prediction of WT progression. Although WSS remains the more
275 sensitive hemodynamic indicator for atherosclerotic disease, *in vivo* WSS measurements are less
276 accurate than measurements of intravascular fluid quantities like HF [31]. Furthermore, future
277 advances in phase-contrast magnetic resonance imaging might extend the feasibility of *in vivo*
278 arterial helical flow quantitative analysis, already demonstrated for large arteries [6,11,32-34], to
279 small vessels like the coronary arteries [17,35-39]. This would allow *in vivo*-based prediction of
280 atherosclerotic disease progression based upon helicity-based descriptors and thereby open a
281 clinical translation of the relationships reported in this study.

282 *Conclusions*

283 This study in coronary arteries confirms a clear association between helical flow, anti-atherogenic
284 wall shear stress patterns and protection from plaque progression over time in an atherosclerotic
285 pig model. In detail, the study confirmed the role of helical blood flow features (in terms of HF
286 intensity) in conditioning WSS luminal distribution, which in turn interacts with the
287 pathophysiology of atherosclerotic plaque formation. Due to its role in determining WSS, HF

288 intensity could act as a practical surrogate marker of low WSS and, thus, as a potential
289 biomechanical predictor of atherosclerotic plaque onset and progression.

290 **Conflict of Interest**

291 The authors state no conflict of interest for the study object of the manuscript. The research was
292 not supported financially by private companies. None of the authors has a financial agreement
293 with peoples or organizations that could inappropriately influence their work.

294 **Financial support**

295 Funding was received from the European Research Council under the European Union's Seventh
296 Framework Programme / ERC Grant Agreement n. 310457.

297 **Author contributions**

298 G.D.N., A.H., C.C, D.G., U.M. and J.J.W.: conception and design of the study; A.H.: acquisition and
299 analysis of in vivo data; G.D.N. and A.M.K.: computational simulation and analysis of simulation
300 data; G.D.N, D.G., C.C., U.M., and J.J.W.: drafting of the manuscript. All authors revised the
301 manuscript critically for important intellectual content and provided final approval for publication.

302 References

- 303 1. Kwak BR, Bäck M, Bochaton-Piallat ML, Caligiuri G, Daemen MJ, Davies PF, Hoefer IE, Holvoet P,
304 Jo H, Krams R, Lehoux S, Monaco C, Steffens S, Virmani R, Weber C, Wentzel JJ, Evans PC.
305 Biomechanical factors in atherosclerosis: mechanisms and clinical implications. *Eur Heart J*
306 2014;35(43):3013-20.
- 307 2. Morbiducci U, Kok AM, Kwak BR, Stone PH, Steinman DA, Wentzel JJ. Atherosclerosis at arterial
308 bifurcations: evidence for the role of haemodynamics and geometry. *Thromb Haemost*
309 2016;115(3):484-92.
- 310 3. Wentzel JJ, Chatzizisis YS, Gijzen FJH, Giannoglou GD, Feldman CL, Stone PH. Endothelial shear
311 stress in the evolution of coronary atherosclerotic plaque and vascular remodelling: current
312 understanding and remaining questions. *Cardiovascular Research* 2012; 96:234-243.
- 313 4. Koskinas KC, Sukhova GK, Baker AB, Papafaklis MI, Chatzizisis YS, Coskun AU, Quillard T, Jonas
314 M, Maynard C, Antoniadis AP, Shi GP, Libby P, Edelman ER, Feldman CL, Stone PH. Thin-Capped
315 Atheromata with Reduced Collagen Content in Pigs Develop in Coronary Arterial Regions
316 Exposed to Persistently Low Endothelial Shear Stress. *Arterioscler Thromb Vasc Biol*
317 2013;33(7):1494-1504.
- 318 5. Stone PH, Saito S, Takahashi S, Makita Y, Nakamura S, Kawasaki T, Takahashi A, Katsuki T,
319 Nakamura S, Namiki A, Hirohata A, Matsumura T, Yamazaki S, Yokoi H, Tanaka S, Otsuji S,
320 Yoshimachi F, Honye J, Harwood D, Reitman M, Coskun AU, Papafaklis MI, Feldman CL,
321 PREDICTION Investigators. Prediction of Progression of Coronary Artery Disease and Clinical
322 Outcomes Using Vascular Profiling of Endothelial Shear Stress and Arterial Plaque
323 Characteristics. The PREDICTION Study. *Circulation* 2012;126:172-181.
- 324 6. Morbiducci U, Ponzini R, Rizzo G, Cadioli M, Esposito A, Montevecchi FM, Redaelli A.
325 Mechanistic insight into the physiological relevance of helical blood flow in the human aorta.
326 An in vivo study. *Biomech Model Mechanobiol* 2011;10:339-355.
- 327 7. Liu X, Sun A, Fan Y, Deng X. Physiological significance of helical flow in the arterial system and
328 its potential clinical applications. *Ann Biomed Eng* 2015;43(1):3-15.

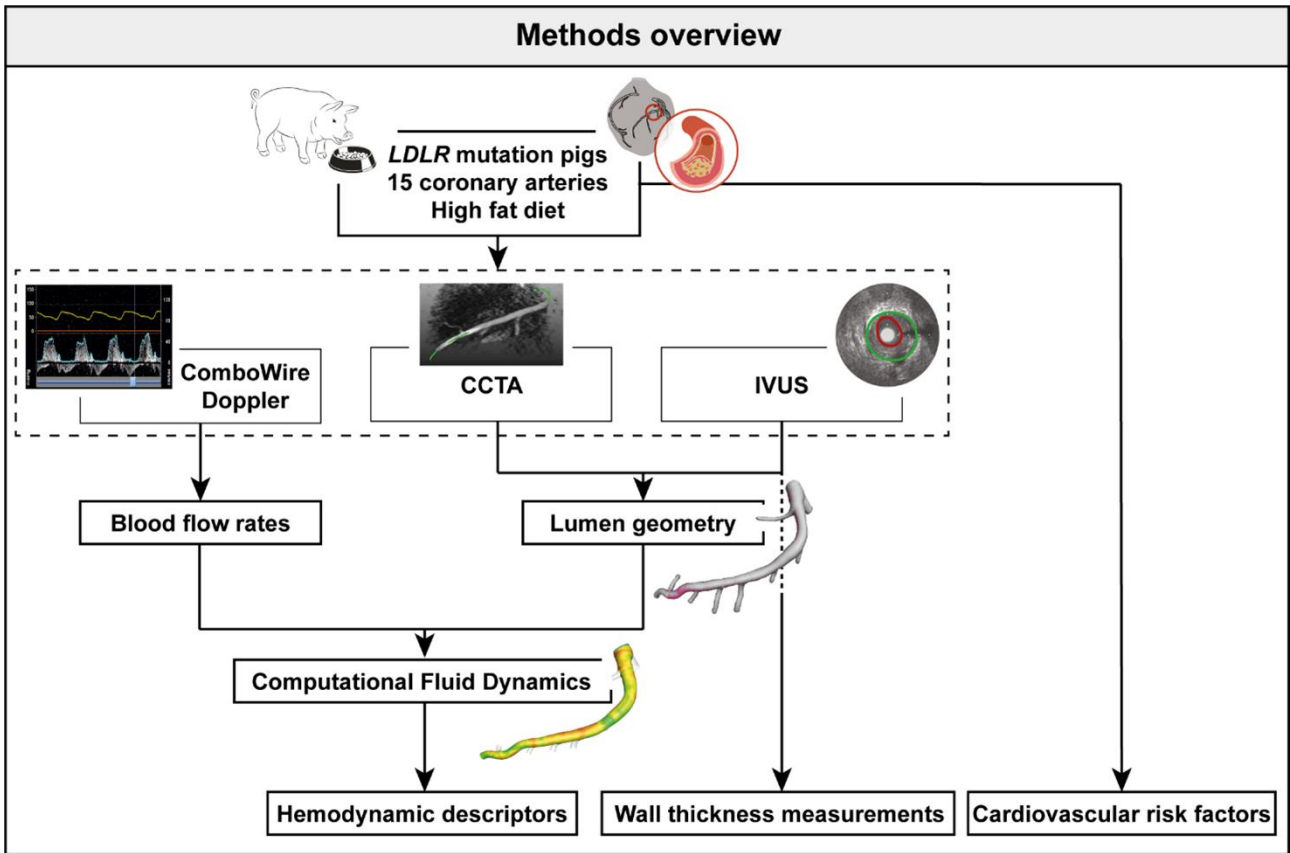
- 329 8. Stonebridge PA, Hoskins PR, Allan PL, Belch JF. Spiral laminar flow in vivo. Clin Sci
330 1996;91(1):17-21.
- 331 9. Stonebridge PA, Suttie SA, Ross R, Dick J. Spiral Laminar Flow: a Survey of a Three-Dimensional
332 Arterial Flow Pattern in a Group of Volunteers. Eur J Vasc Endovasc Surg 2016;52(5):674-680.
- 333 10. Liu X, Pu F, Fan Y, Deng X, Li D, Li S. A numerical study on the flow of blood and the transport of
334 LDL in the human aorta: the physiological significance of the helical flow in the aortic arch. Am J
335 Physiol Heart Circ Physiol 2009;297:H163-H170.
- 336 11. Morbiducci U, Ponzini R, Rizzo G, Cadioli M, Esposito A, De Cobelli F, Del Maschio A,
337 Montevecchi FM, Redaelli A. In vivo quantification of helical blood flow in human aorta by time-
338 resolved three-dimensional cine phase contrast MRI. Ann Biomed Eng 2009;37:516-531.
- 339 12. Morbiducci U, Ponzini R, Gallo D, Bignardi C, Rizzo G. Inflow boundary conditions for image-
340 based computational hemodynamics: impact of idealized versus measured velocity profiles in
341 the human aorta. J Biomech 2013;46:102-109.
- 342 13. Gallo D, Steinman DA, Bijari PB, Morbiducci U. Helical flow in carotid bifurcation as surrogate
343 marker of exposure to disturbed shear. J Biomech 2012;45:2398-2404.
- 344 14. Gallo D, Steinman DA, Morbiducci U. An Insight into the Mechanistic Role of the Common
345 Carotid Artery on the Hemodynamics at the Carotid Bifurcation. Ann Biomed Eng 2015;43:68.
- 346 15. Gallo D, Bijari PB, Morbiducci U, Qiao Y, Xie Y, Etesami M, Haabets D, Lakatta EG, Wasserman
347 BA, Steinman DA. Segment-specific associations between local haemodynamic and imaging
348 markers of early atherosclerosis at the carotid artery: an in vivo human study. J R Soc Interface
349 2018;15:20180352.
- 350 16. De Nisco G, Kok AM, Chiastra C, Gallo D, Hoogendoorn A, Migliavacca F, Wentzel JJ, Morbiducci
351 U. The Atheroprotective Nature of Helical Flow in Coronary Arteries. Ann Biomed Eng
352 2019;47(2):425-438.
- 353 17. Markl M, Schnell S, Wu C, Bollache E, Jarvis K, Barker AJ, Robinson JD, Rigsby CK. Advanced flow
354 MRI: emerging techniques and applications. Clin Radiol 2016;71(8):779-95.

- 355 18. Hoogendoorn A, Kok AM, Hartman EMJ, De Nisco G, Casadonte L, Chiastra C, Coenen A,
356 Korteland SA, Van der Heiden K, Gijsen FJH, Duncker DJ, van der Steen AFW, Wentzel JJ,
357 Multidirectional wall shear stress promotes advanced coronary plaque development –
358 comparing five shear stress metrics. *Cardiovasc Res* 2019;cvz212
359 <https://doi.org/10.1093/cvr/cvz212>.
- 360 19. National Research Council (US). Committee for the Update of the Guide for Care and Use of
361 Laboratory Animals, *Guide for the Care and Use of Laboratory Animals* (8th ed.). Washington,
362 DC: National Academies Press (US), 2011.
- 363 20. Huo Y, Kassab GS. Intraspecific scaling laws of vascular trees. *J R Soc Interface* 2012;9(66):190-
364 200.
- 365 21. Morbiducci U, Ponzini R, Grigioni M, Redaelli A. Helical flow as fluid dynamic signature for
366 atherogenesis in aortocoronary bypass. A numeric study. *J Biomech* 2007;40:519-534.
- 367 22. Morbiducci U, Gallo D, Cristofanelli S, Ponzini R, Deriu MA, Rizzo G, Steinman DA. A rational
368 approach to defining principal axes of multidirectional wall shear stress in realistic vascular
369 geometries, with application to the study of the influence of helical flow on wall shear stress
370 directionality in aorta. *J Biomech* 2015;48(6):899-906.
- 371 23. Malek AM, Alper SL, Izumo I. Hemodynamic shear stress and its role in atherosclerosis. *JAMA*.
372 1999;282:2035-2042.
- 373 24. Chatzizisis YS, Coskun AU, Jonas M, Edelman ER, Feldman CL, Stone PH. Role of Endothelial
374 Shear Stress in the Natural History of Coronary Atherosclerosis and Vascular Remodeling. *J Am*
375 *Coll Cardiol* 2007;49:2379-93.
- 376 25. Fox B, James K, Morgan B, Seed WA. Distribution of fatty and fibrous plaques in young human
377 coronary arteries. *Atherosclerosis*. 1982;41:337-347.
- 378 26. Nakashima T, Iwanaga Y, Nakaura Y. Pathologic study of hypertensive heart. *Acta Pathologica*
379 *Japonica*. 1964;14(1):129-141.
- 380 27. Nakashima T, Tashiro T. Early morphologic stage of human coronary atherosclerosis. *Kurume*
381 *Med J*. 1968;15(4):235-42.

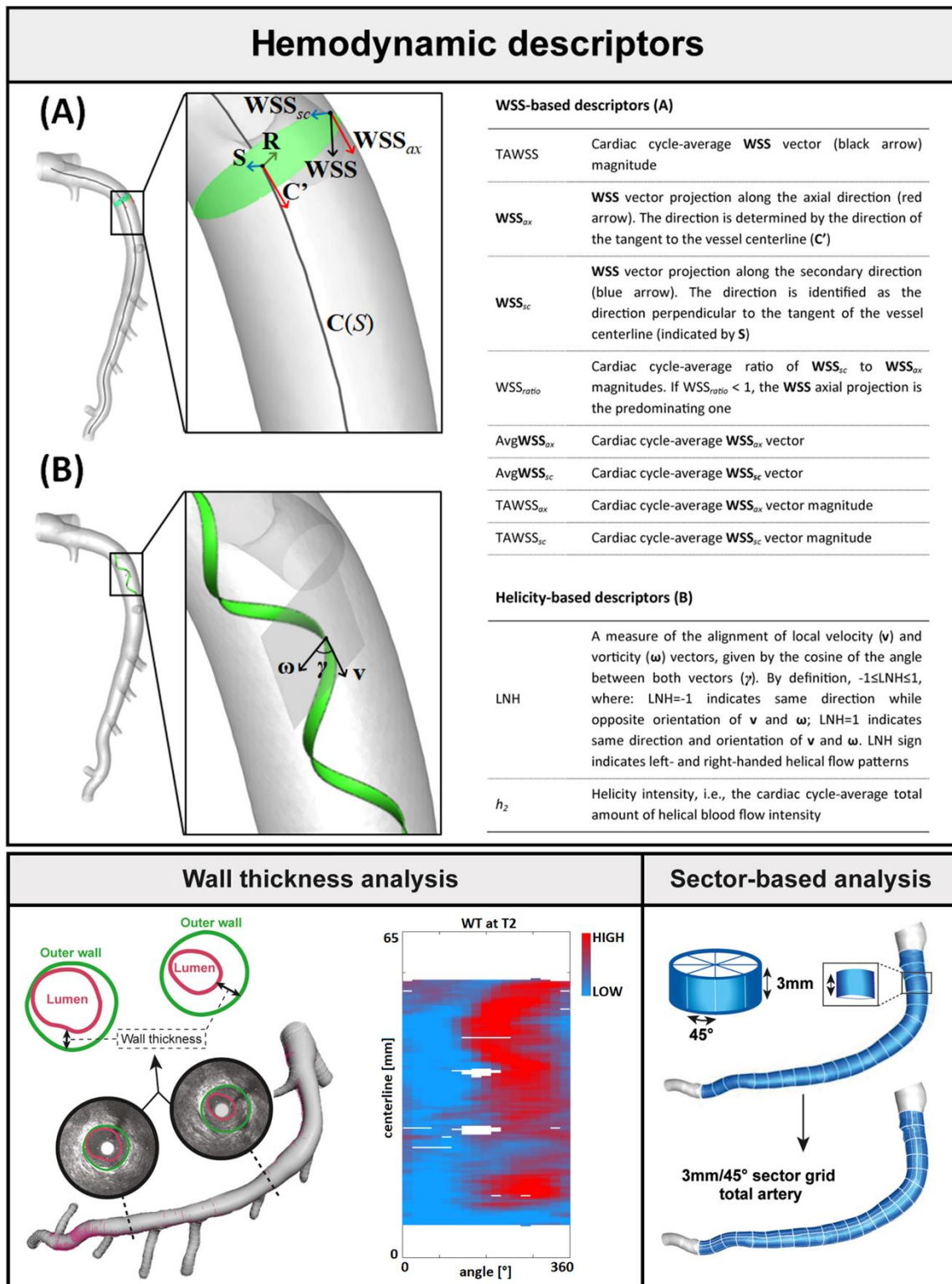
- 382 28. Sabbah HN, Walburn FJ, Stein PD. Patterns of flow in the left coronary artery. *J Biomech Eng.*
383 1984;106(3):272-9.
- 384 29. Torii R, Keegan J, Wood NB, Dowsey AW, Hughes AD, Yang GZ, Firmin DN, Thom SA, Xu XY. MR
385 image-based geometric and hemodynamic investigation of the right coronary artery with
386 dynamic vessel motion. *Ann Biomed Eng* 2010;38:2606-2620.
- 387 30. Winkel LC, Hoogendoorn A, Xing R, Wentzel JJ, Van der Heiden K. Animal models of surgically
388 manipulated flow velocities to study shear stress-induced atherosclerosis. *Atherosclerosis.*
389 2015;241:100-110.
- 390 31. Frydrychowicz A., Berger A, Munoz Del Rio A, Russe MF, Bock J, Harloff A, Markl M.
391 Interdependencies of aortic arch secondary flow patterns, geometry, and age analysed by 4-
392 dimensional phase contrast magnetic resonance imaging at 3 Tesla. *Eur. Radiol.*
393 2012;22(5):1122-30.
- 394 32. Harloff A, Albrecht F, Spreer J, Stalder AF, Bock J, Frydrychowicz A, Schöllhorn J, Hetzel A,
395 Schumacher M, Hennig J, Markl M. 3D blood flow characteristics in the carotid artery
396 bifurcation assessed by flow-sensitive 4D MRI at 3T. *Magn Reson Med* 2009;61(1):65-74.
- 397 33. Schäfer M, Barker AJ, Kheyfets V, Stenmark KR, Crapo J, Yeager ME, Truong U, Buckner JK,
398 Fenster BE, Hunter KS. Helicity and Vorticity of Pulmonary Arterial Flow in Patients With
399 Pulmonary Hypertension: Quantitative Analysis of Flow Formations. *J Am Heart Assoc.*
400 2017;6(12):e007010.
- 401 34. Oechtering TH, Sieren MM, Hunold P, Hennemuth A, Huellebrand M, Scharfschwerdt M,
402 Richardt D, Sievers HH, Barkhausen J, Frydrychowicz A. Time-resolved 3-dimensional magnetic
403 resonance phase contrast imaging (4D Flow MRI) reveals altered blood flow patterns in the
404 ascending aorta of patients with valve-sparing aortic root replacement. *J Thorac Cardiovasc*
405 *Surg.* 2019;S0022-5223(19)30773-1.
- 406 35. Brandts A, Roes SD, Doornbos J, Weiss RG, de Roos A, Stuber M, Westenberg JJ. Right coronary
407 artery flow velocity and volume assessment with spiral k-space sampled breathhold velocity-
408 encoded MRI at 3 tesla: accuracy and reproducibility. *J Magn Reson Imaging.* 2010;31(5):1215-
409 1223.

- 410 36. Keegan J, Gatehouse PD, Mohiaddin RH, Yang GZ, Firmin DN. Comparison of spiral and FLASH
411 phase velocity mapping, with and without breath-holding, for the assessment of left and right
412 coronary artery blood flow velocity. *J Magn Reson Imaging*. 2004;19(1):40-49.
- 413 37. Johnson K, Sharma P, Oshinski J. Coronary artery flow measurement using navigator echo gated
414 phase contrast magnetic resonance velocity mapping at 3.0 T. *J Biomech*. 2008;41(3):595-602.
- 415 38. Jahnke C, Manka R, Kozerke S, Kozerke S, Schnackenburg B, Gebker R, Marx N, Paetsch I.
416 Cardiovascular magnetic resonance profiling of coronary atherosclerosis: vessel wall
417 remodelling and related myocardial blood flow alterations. *Eur Heart J Cardiovasc Imaging*.
418 2014;15(12):1400-1410.
- 419 39. Nagel E, Thouet T, Klein C, Schalla S, Bornstedt A, Schnackenburg B, Hug J, Wellnhofer E, Fleck
420 E. Noninvasive determination of coronary blood flow velocity with cardiovascular magnetic
421 resonance in patients after stent deployment. *Circulation*. 2003;107(13):1738-1743.

422

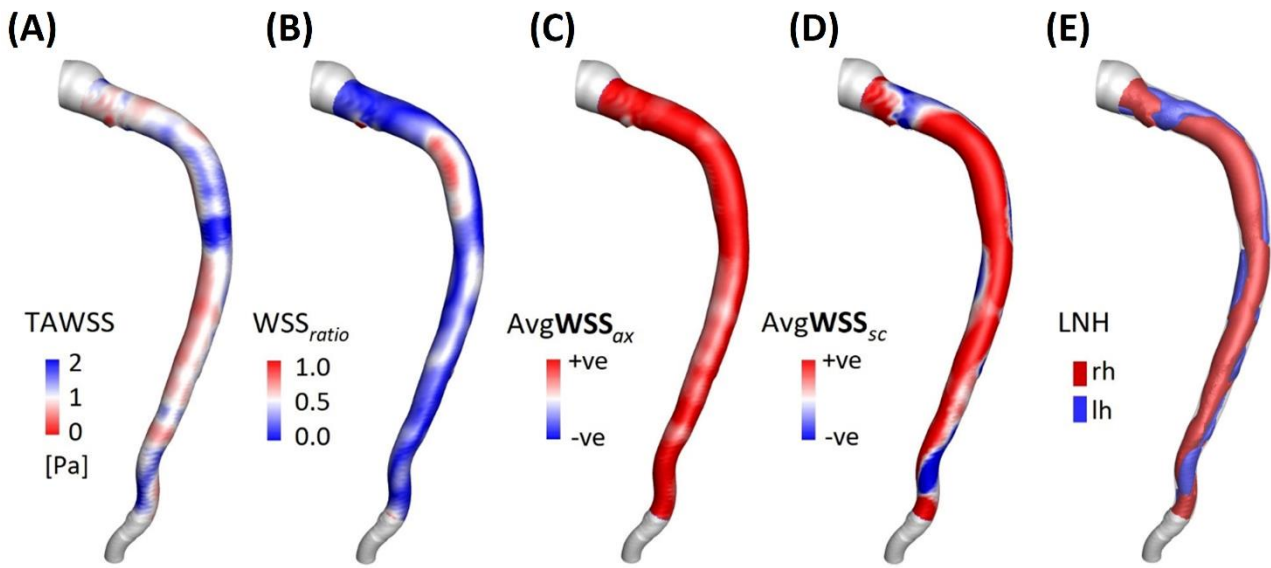


424
 425 **Figure 1. Schematic diagram of the study design, showing how imaging data contribute to define**
 426 **vessel geometry and hemodynamic variables.** *LDRL*: low-density lipoprotein receptor; CCTA:
 427 coronary computed tomography angiography; IVUS: intravascular ultrasound.

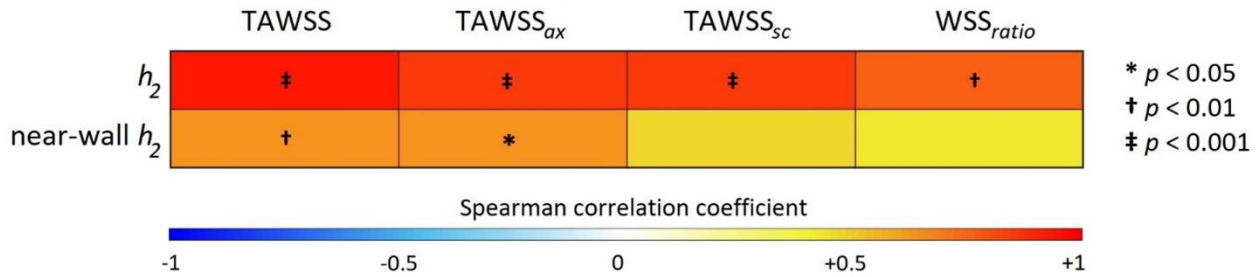


428
429
430
431
432
433
434
435
436
437
438
439
440

Figure 2. Methodology of hemodynamic descriptors and wall thickness (WT) assessment and analysis. Hemodynamic descriptors panel - Figure (A): example of **WSS** vector acting in a generic point at the luminal surface. Its axial (**WSS_{ax}**) and secondary (**WSS_{sc}**) components are also displayed. **C(S)**: vessel centerline; **C'**: vector tangent to the centerline; **R**: vector perpendicular to **C'** directed from the centerline to the generic point at the arterial surface; **S**: vector orthogonal to vectors **R** and **C'**. Table (A): WSS-based descriptors involved in the analysis. A short caption for each descriptor is provided. Figure (B): example of the helical-shaped trajectory described by an element of blood moving within the coronary artery. **gamma** is the angle between local velocity (**v**) and vorticity (**omega**) vectors (**LNH** = $\cos(\gamma)$). Table (B): helicity-based descriptors involved in the analysis. A short caption for each descriptor is provided. **Wall thickness analysis panel** - Example of lumen (pink contour) and vessel outer wall (green contour) segmentation on two IVUS frames of an explanatory case. The obtained 2D distribution of WT at T2 is also shown. The angle indicates the circumferential direction around the arterial lumen. The top of the graph is the proximal region and the bottom of the graph is the distal region of the artery. **Sector-based analysis panel** - Example of IVUS-imaged segment (blue colored) region in 3mm/45 degrees luminal sectors for an explanatory case.

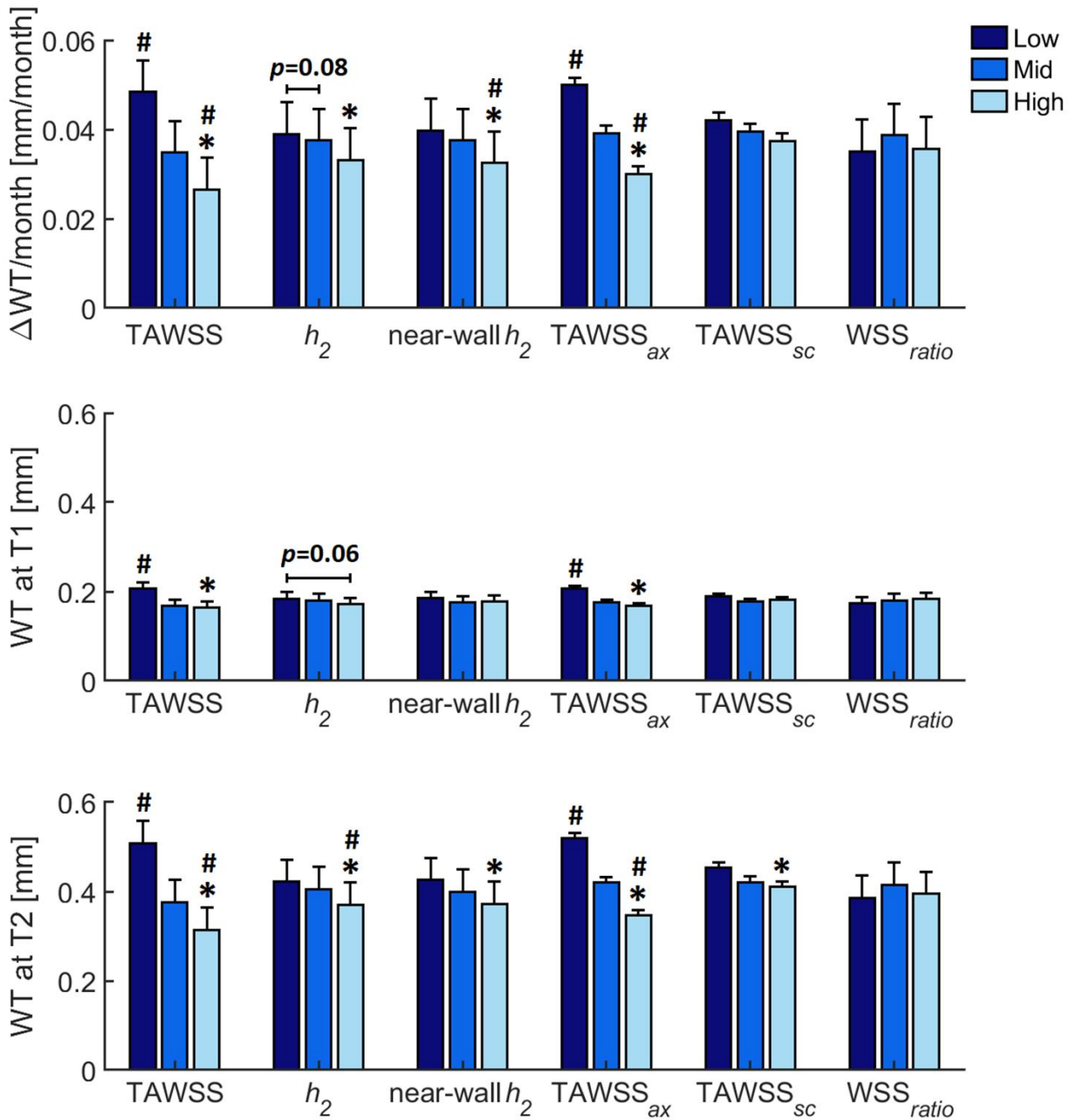


(F)

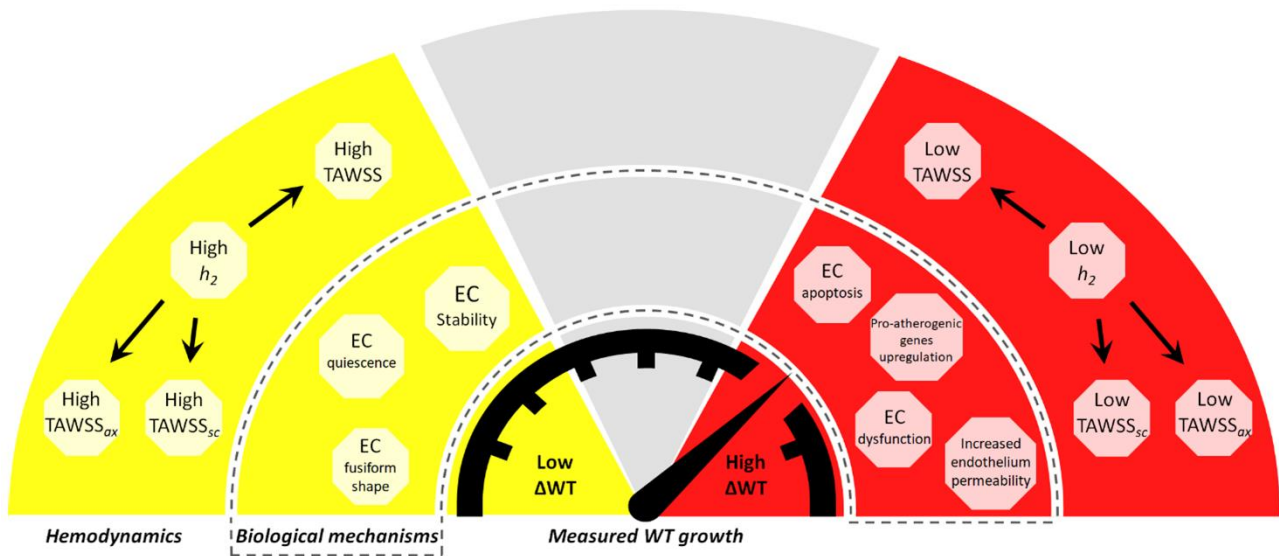


441
442
443
444
445
446
447
448
449
450
451
452

Figure 3. Coronary hemodynamics: general observations and link between hemodynamic variables. (A)-(D) WSS-based descriptors distribution at the luminal surface of a representative LAD coronary artery (a) (see Figure S1 of the Supplementary Materials). For the same explanatory case, visualization of LNH cycle-average isosurfaces is also provided in panel (E). For TAWSS (WSS_{ratio}), the low (red) and high (blue) values are indicated. For cycle-average axial ($AvgWSS_{ax}$) WSS vector projections, colors identify the forward (red) and backward (blue) flow direction, respectively. As for LNH, also for the cycle-average secondary ($AvgWSS_{sc}$) WSS vector projections blue and red colors identify the left and right-handed direction, respectively. +ve: positive; -ve: negative; rh: right-handed; lh: left-handed. (F) Spearman correlation coefficients between WSS-based and helicity-based descriptors. The average value of the hemodynamic descriptors for each individual case was considered. For statistically significant relations, p values are also reported.



453
 454 **Figure 4. Link between hemodynamic variables and increase in wall thickness.** Relationship
 455 between baseline (T1) hemodynamic descriptor levels and 1) estimated plaque growth per month
 456 (top panel), 2) WT at T1 (middle panel), and 3) WT at T2 (bottom panel). Estimated mean and
 457 standard error of the mean (SEM) values are reported. The hemodynamic descriptors were divided
 458 in low (dark blue bars), mid (blue bars) and high (light blue bars) tertiles per artery. The average
 459 value of the hemodynamic descriptors and WT measurements in the 3mm/45 degrees sectors was
 460 considered. * $p < 0.05$ compared to low tertile, # $p < 0.05$ compared to the mid tertile of all
 461 parameters.



462
463
464

Figure 5. Schematic of the main findings of the study and the relationship with biological mechanisms related to atherosclerosis